Molecular dynamics study on stiffness and ductility in chitin–protein composite

Citation: Yu, Zechuan, and Denvid Lau. "Molecular Dynamics Study on Stiffness and Ductility in Chitin–protein Composite." Journal of Materials Science 50, no. 21 (July 21, 2015): 7149–7157.

As Published: http://dx.doi.org/10.1007/s10853-015-9271-y

Publisher: Springer US

Persistent URL: http://hdl.handle.net/1721.1/103325

Version: Author's final manuscript: final author's manuscript post peer review, without publisher's formatting or copy editing

Molecular dynamics study on stiffness and ductility in chitin-protein composite

Zechuan Yu[a] (Email: zec.yui@my.cityu.edu.hk)

Denvid Lau[a,b,*] (Email: denvid@mit.edu)

[a] Department of Architecture and Civil Engineering, City University of Hong Kong, Hong Kong, China.

[b] Department of Civil and Environmental Engineering, Massachusetts Institute of Technology, Cambridge, MA, USA.

[*] Corresponding author, tel: 852-34426829

Abstract: Chitin-protein composite is the structural material of many marine animals including lobster, squid and sponge. The relationship between mechanical performance and hierarchical nanostructure in those composites attracts extensive research interests. In order to study the molecular mechanism behind, we construct atomistic models of chitin-protein composite and conduct computational tensile tests through molecular dynamics simulations. The effects of water content and chitin fiber length on the stiffness are examined. The result reveals the detrimental effect on the stiffness of chitin-protein composite due to the presence of water molecules. Meanwhile, it is found that the chitin-protein composite becomes stiffer as the embedded chitin fiber is longer. As the tensile deformation proceeds, the stress-strain curve features a saw-tooth appearance, which can be explained by the interlocked zigzag nanostructure between adjacent chitin fibers. These interlocked sites can sacrificially break for energy dissipation when the system undergoes large deformation, leading to an improvement of ductility.

Keywords: chitin; critical length; elastic modulus; molecular dynamics; nanostructure

1. Introduction

Chitin is a most abundant biological polymer in the kingdom of animals, especially marine animals and insects [1]. Crystalline chitin fiber possesses good mechanical properties so that it can serve as a load-bearing scaffold for the entire bio-composite material [2], in which the other component is usually protein. The remarkable affinity [3] between chitin and protein is probably one of the main reasons why such composite system can be readily found in nature. Lots of biological materials, such as the exoskeleton of sponges, the cuticles of crustaceans and insects, the beaks of squids and the fangs of spiders, are made of chitin and protein [4-8]. Those chitin-protein materials present diverse mechanical behaviors and serve for multiple functions among different species and even among different parts of the body of one species like lobster [9-11]. With the composition of lobster cuticle resolved, it is shown that the diverse mechanical performance could arise from adaptive variations in composition [12]. Moreover, it is found that the lobster cuticles are constructed in a hierarchical manner and such hierarchical structure plays a critical role in tuning the mechanical properties [13,14]. Multi-scale modeling techniques have been used to investigate the molecular mechanics at chitin-protein interface and illustrate the hierarchical architectures formed by chitin fibers, protein sheets and mineral [15-18]. Viewing at different length scales, one should notice that the chitin-protein composites are quite different in mechanical performance and material morphology. In such chitin-protein systems the hierarchical structures and the resulting mechanical properties attract extensive research interests [19-22]. Though, most of chitin-related studies reside on either extremely small length scale (~ several Å) or micro-scale (~ 1 μm), whereas the studies on the nanostructures (with the size of

around 10 nm) formed in the chitin-protein composite and how the nanostructures is related to the mechanical properties are limited. In order to study the molecular mechanism behind the mechanical properties, we design an atomic model representing nanostructure of the chitin-protein composite and conduct investigations on its mechanical performance. The tension-shear chain (TSC) model, which is firstly used to describe the structure of bone and is later found to be a generic model for biological nanocomposites [23-25], provides a possible pattern to combine chitin fibers and protein sheets at the length scale of tens of nanometer. The constituents of TSC model are the hard inclusions and the amorphous matrix, which are either too brittle or too flexible to form stable materials [26]. However, in TSC model, their astute combination in a staggered manner can optimize both the strength and the stiffness of the composite [23,27]. Mechanical properties of TSC-type composites are closely related to the geometry of the hard inclusions (the length of chitin fiber in our case) as well as the interface between the hard inclusions and the amorphous matrix (the chitin-protein interface) [25].

Recent studies have shown that the dimension of constituent in biological composites is closely related to their mechanical properties [28-30]. For instance, the fracture energy of cellulose nanocrystals (CNCs) is maximized at certain width (ranging from 6.2–7.3 nm) and thickness (ranging 4.8–5.6 nm) [28]. In silk material, properly sized protein crystals can offer optimal load bearing capacity [29,30]. In bone, mineral particles with the critical size become insensitive to defects and have strength close to theoretical limit [24]. In the structures of bone and shell, a theoretical study has pointed out the existence of characteristic length of mineral constituents that accounts for the optimized stress transfer efficiency [31]. Considering that the modelled chitin-protein system shares a similar tension-shear chain structure with that of bone and shell, we expect that mechanical properties of the chitin-protein composite could be critically linked

with length of the embedded chitin fiber. Meanwhile, as the modelled composite encompasses many chitin-protein interfaces, effect from water could play an important role in tuning the mechanical properties, like many materials with bilayer interfaces [15,17,32,33]. At the chitin-protein interface, water molecules interfere in the bilayer connection and reduce the adhesion strength [15]. However, the hydration effect towards the mechanical properties of the entire chitin-protein composite remains undiscovered.

As introduced above, the length of embedded chitin fibers and the presence of water molecules may influence mechanical properties of the chitin-protein composite. In this paper we are answering the question about how these two factors control the stiffness of the chitin-protein composite. We firstly construct an atomistic model of chitin-protein composite following the design of tension-shear chain model. Then, we perform computational tensile testing to obtain elastic modulus and strength of chitin-protein composites with varied chitin fiber length in dry and wet environments. Through analyzing of the stress-strain curves during large deformation, we examine the dependence of ductility towards the length of chitin fiber. A special remark in the stress-strain curve is noted, which could be related to energy dissipation and stress relaxation mechanisms in the chitin-protein composite system.

2. Method

2.1. Model construction

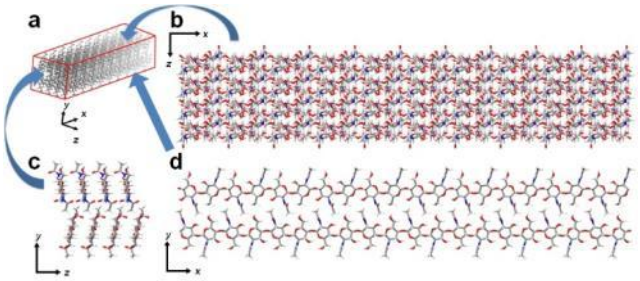

Fig. 1 a 3-d snapshot of a single chitin fiber with all atoms in gray. **b c d** Snapshots of the chitin fiber from three angles of view, with carbon atom, oxygen atom, nitrogen atom and hydrogen atom in gray, red, blue and white respectively

Chitin (β-(1→4)-N-acetyl-D-glucosamine) is an acetylated polysaccharide akin to cellulose. Similar to cellulose crystallization, chitin also adopts several types of crystalline structures including α-, β- and γ-chitin. Among these crystalline chitin structures, α-chitin accounts for the major amount [19]. Previous studies have resolved the conformation of α-chitin unit cell [35,19]. Replication of this unit cell along the backbone direction results in a pair of antiparallel chains. Four pairs of antiparallel chains constitute one chitin fiber with a cross section of 2×2 nm^2. Snapshots of such chitin fiber show the details of the model in Fig. 1. Snapshots are captured using VMD [36].

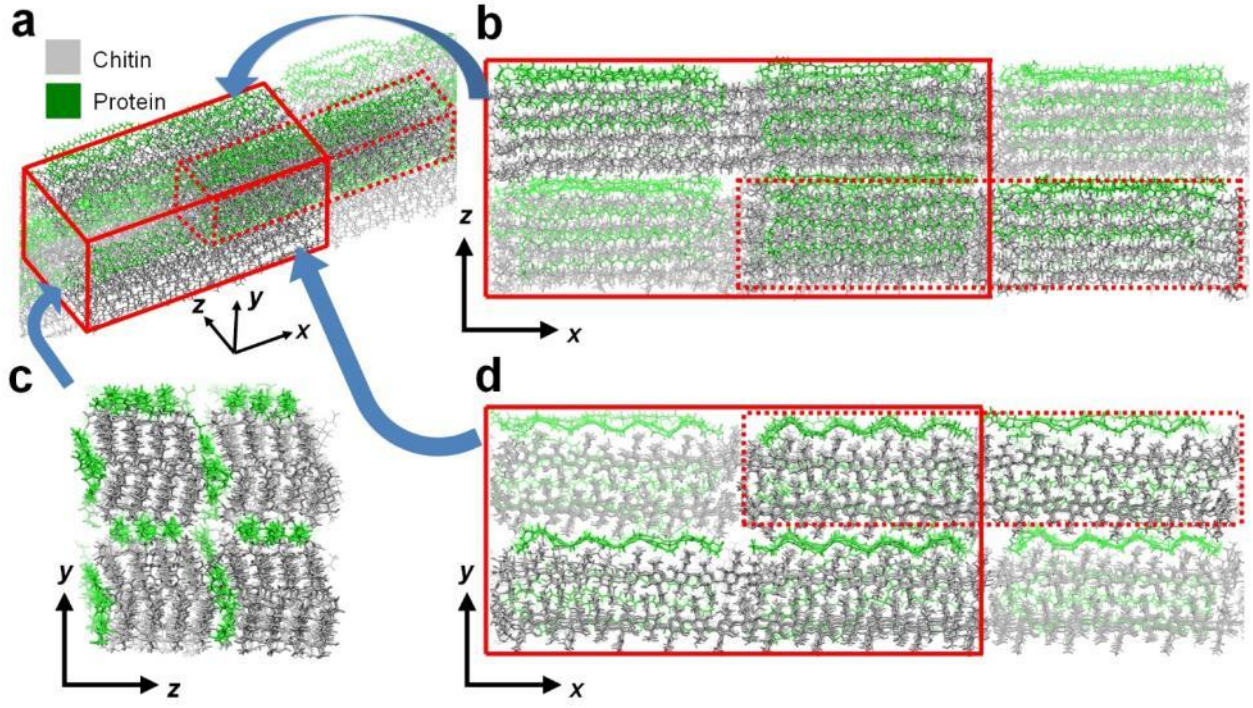

Fig. 2 a Three-dimensional snapshot of chitin-protein composite consisting of four chitin-protein fibers. The solid lines point out one repeating unit, the dashed lines point out one chitin-protein fiber. **b c d** Snapshots of the chitin-protein fiber viewing from three angles

Protein sheet is a three-strand β-sheet composed of 40 glycine. The β-sheet is 2 nm in width and can cover the lateral section of one chitin fiber. Glycine is the dominant kind of amino acids in natural chitin-based materials such as squid beaks [7]. Despite that the detailed information about the protein sequence is lacking, glycine is chosen to construct the protein as a simplified treatment, which is able to capture the basic features of protein backbone without any side-chain. The C- and N-termini of these proteins are in neutral state (-COOH and -NH_2). Two pieces of protein β-sheets covering the lateral sections, together with one chitin fiber embedded inside, constitute one chitin-protein fiber as outlined by dashed lines in Fig. 2a. The thickness of the protein sheets and chitin fibers are around 0.5 nm and 2 nm respectively. As a result, the fraction volume of the chitin fibers is 0.64. Chitin fibers and protein sheets form structure like tension-shear chain model [23], where chitin fibers act as hard inclusions and proteins are soft matrices wrapping around. Four chitin-protein fibers assembly in an interconnected and staggered manner to form the chitin-protein composite, as shown in Fig. 2b, c d. These snapshots demonstrate the staggered assemblage from three view angles. Along the backbone direction (x axis), the length of simulation box is set to the length of one chitin-protein fiber, as outlined by the solid lines in Fig. 2a, where the opaque part is the original image and the relatively transparent part is the periodic image. Hence, the constitutively interconnected chitin-protein fibers are modeled and simulated under the periodic boundary condition. We vary the length of embedded chitin fibers in chitin-protein composite and construct 7 samples with the fiber length ranging from 5 nm to 35 nm, as the 5-35 nm range is suggested by experimental study [7]. In the 5 nm-long chitin fiber case the chitin-protein model contains 11000 atoms and the number of atoms are almost proportional to the length of chitin fiber in larger systems.

2.2. Simulation Details

Large-scale Atomic/Molecular Massively Parallel Simulator (LAMMPS) is the platform for performing molecular dynamics simulations [37]. CHARMM36 additive all-atom biomolecule force field is used to define the atomic potential of α-chitin fiber and the protein β-sheet [38,39]. The interaction between chitin and protein encompasses van der Waals and Columbic forces. Following the standard CHARMM force field principles, there is no specific definition for hydrogen bonds, instead, the hydrogen-bond effect is taken into consideration by CHARMM force field via specific assignment of atomic charges. Therefore, the number of hydrogen bonds can be regarded as a qualitative indicator of the interaction strength [15]. The criteria for detecting hydrogen bonds are set to that the cutoff of donor-acceptor distance is 4 Å and the donor-hydrogen-acceptor angle is set to 35°. The cutoff of non-bonded interactions is 10 Å. The SHAKE algorithm is applied to fix hydrogen-related energy terms. The particle-particle particle-mesh (PPPM) method is used to compute long-range Coulomb interactions. Periodic boundary condition is set to all three directions.

The equilibration procedures follow a previous study [40]. Firstly, the system energy is minimized using conjugate gradient algorithm. Next, the system is heated from 50 K to 300 K in 200 ps in NVT ensemble. The Nosé-Hoover thermostat and anisotropic barostat are applied to control the temperature and the pressure, which are set to 300 K and 1 atm respectively. The system is then equilibrated for 1 ns in NPT ensemble. The standard deviation of RMSD during the latter 0.5 ns is less than 0.2, proving that the equilibration has been achieved after this set of simulation procedures. After equilibration, we immerse these chitin-protein composite models into water box. Water molecules constitutes around 14.6% in weight of the entire system. For the 5 nm-long chitin fiber case, the water box consists of 4400 water molecules, while in larger systems the number of water molecules are proportional to the chitin fiber length. In Fig. 3, we

present the periodic images of the equilibrated systems and plot a contour of hydrogen-bond distribution. Tensile tests are performed in both dry and wet cases. The tensile test with a smaller strain rate is conducted to obtain the elastic modulus of the bonded system. The strain rate is 0.002 per nanosecond and every 500 ps the size of the simulation box in the backbone direction is enlarged by 0.001. Using this setting, the system undergoes a 500-ps equilibration at each strain state so that the rate-dependent effect can be minimized [15]. Within each 500 ps, the stress average over the latter 250 ps is calculated as the stress at this strain. The tensile test lasts for 10 ns. As a result, the strain will eventually reach to 0.02. Considering that the strain rate is a general concern in molecular dynamics studies, we have also performed a series of tensile tests with strain rate ranging from high (0.2/ns) to low (0.0005/ns) values and simulations with the strain rate lower than 0.005/ns can provide comparable estimations on elastic modulus. A larger-strain tensile test is performed and stress-strain response of the system to large deformation is obtained. The strain rate increases to 0.05 per nanosecond and the maximum strain goes up to 0.5 for the large deformation.

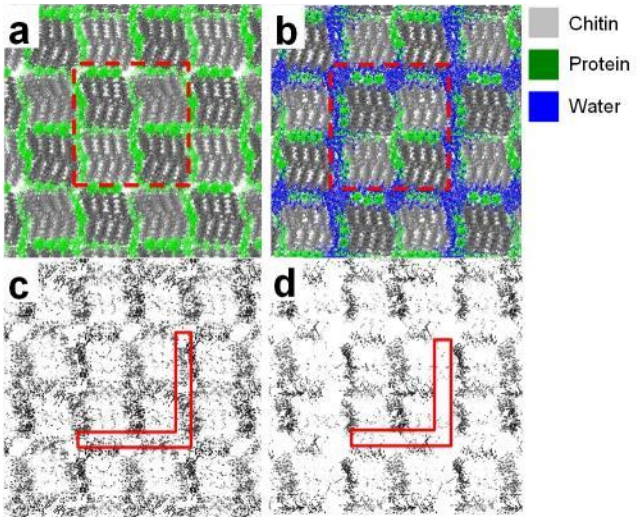

Fig. 3 a b Snapshots showing the cross section of the periodic chitin-protein systems without and with water respectively. The dashed red rectangle outlines the original image and the surrounding parts are periodic images. **c d** Contour plots of distribution of hydrogen bonds formed between chitin and protein in dry and wet cases respectively. Dry sample contains more hydrogen bonds than wet sample does, especially in the region outlined by red lines

3. Results

3.1. The elastic moduli of chitin and chitin-protein composite

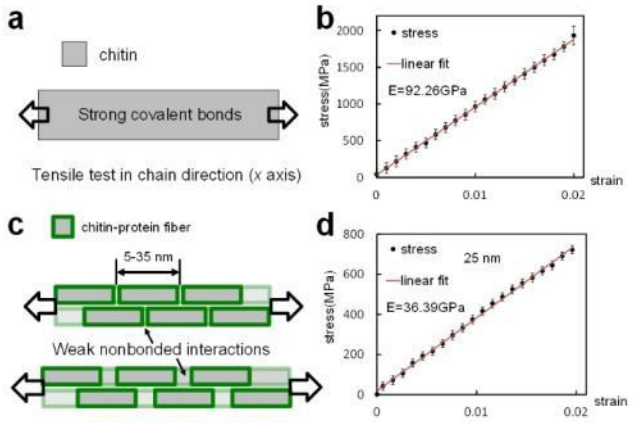

Fig. 4 a The scheme showing the tensile test on chitin fiber. **b** The stress-strain curve for chitin fiber. **c** The scheme of tensile test on chitin-protein composite. **d** The stress-strain curve for chitin-protein composite with 25 nm-long chitin fiber embedded (without water molecules)

Tensile test with small strain rate is conducted on crystalline chitin fiber as schematically shown in Fig. 4a. The stress-strain relationship and the linear fitting series are plotted in Fig. 4b. The backbone elastic modulus of α-chitin fiber is 92.26 GPa. Such high elastic modulus is resulted from the strong covalent bonds that connect chitin monomers tightly along the backbone direction, making chitin fiber the reinforcing phase in chitin-protein composite materials. The result is comparable to the results from other numerical studies [15,16].

Tensile deformation tests are conducted on chitin-protein composites with varied chitin fiber lengths (from 5 nm to 35 nm). We have also performed steered molecular dynamics simulations

(which can be regarded as load-control mechanical test) in 10 nm cases and found that the results from both simulations are close. The stress-strain curves yield the value of elastic modulus. As shown in Fig. 4c, relatively weak non-bonded interactions are responsible for the stress. The stress-strain curve and the linear fitting are plotted in Fig. 4b and d. For the chitin-protein composite with 25-nm long chitin fiber embedded, the elastic modulus is 36.39 GPa, lower than the modulus of pure chitin fiber. Because the dominant interactions for adjacent chitin-protein components are relatively weak van der Waals and Coulomb interactions instead of the strong covalent bonds, it is reasonable that the composite system possesses lower elastic modulus than that of pure chitin fiber. The elastic moduli of chitin-protein composites with varied chitin fiber length are shown in Fig. 5. In dry cases, the elastic moduli range from around 15 GPa to 35 GPa, while in wet cases the range is from 10 GPa to 25 GPa, around 10 GPa lower compared to the dry cases.

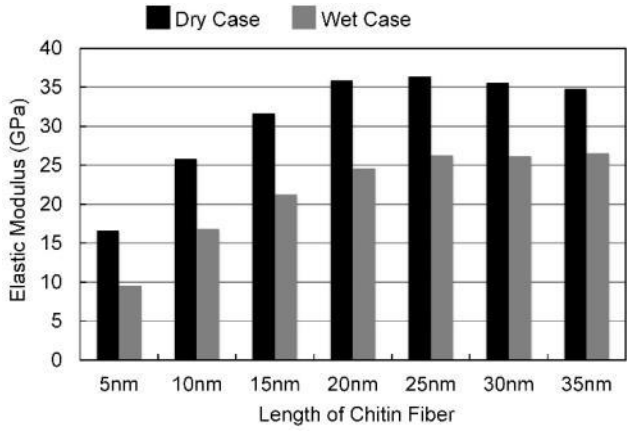

Fig. 5 Bar chart presenting the elastic moduli of all chitin-protein composites under dry (bars in black) and wet (bars in gray) conditions

3.2. The cycling stress-strain curves in large deformation

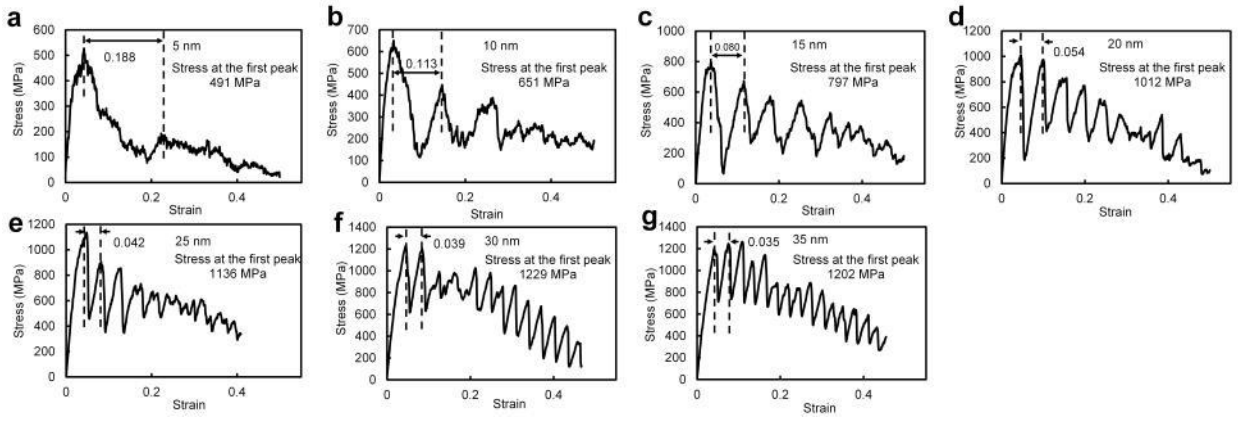

Fig. 6 a-g The stress-strain curves of chitin-protein composite subjected to large deformation. Dashed lines point out the spacing between adjacent peak.

While small strain tensile tests provide accurate result of elastic modulus, the large strain (up to 0.5) tensile tests give more complete information about strength (stress at the first peak) and ductility of chitin-protein composite. We obtain the stress-strain curves via large-strain tensile testing. As shown in Fig. 6, the stress-strain curves feature a cycling increase-decrease appearance, *i.e.*, the stress increases to the peak, quickly drops down and then increases again, repeating for several turns. When chitin fiber length is smaller than 20 nm, the stress falls to a low value after the first peak, whereas in the cases of 25 nm, 30nm and 35 nm, the stress maintains after several increase-decrease cycles. Such phenomenon indicates that the ductility of chitin-protein composite benefits from the increased length of embedded chitin fibers. Noticing the saw-tooth appearance, we define the interval between neighbor peaks as "spacing strain", as displayed in the Fig. 6. The spacing strain decreases as the chitin fiber length increases, suggesting a reciprocal relationship. The product of strain times the chitin fiber length may correspond to the dimension of a special nanostructure formed by interlocked chitin fibers, which will be discussed in section 4.2.

4. Discussion

4.1. The dependence of stiffness on chitin fiber length and water

The elastic moduli of chitin-protein composite range from 15-35 GPa. Previous study has defined a representative volume element (RVE) of chitin-protein fiber and derived a reasonable elastic modulus (around 16 GPa) from Mori-Tanaka scheme [16,41]. In our models, elastic moduli are equal to or higher than 16 GPa. The difference mainly originates from the difference in the volume fraction of chitin fiber. According to the tension-shear chain model [25], elastic modulus of the composite (E) is a function of volume fraction (Φ), stiffness (E_m) and length (L) of the hard inclusion (the chitin fiber in the current study) as shown in Eq. (1). Original tension-shear chain formula encompasses more variables, which is grouped into a constant term α here because the only varied parameter among our chitin-protein samples is the chitin fiber length. We simplify the formula by using the term α combining extra variables in order to put the focal point on the fiber length (L).

$$\frac{1}{E} = \frac{1}{\Phi E_m} + \frac{\alpha}{L^2} \qquad (1)$$

The present atomistic model contains more chitin fiber (volume fraction is 0.64) compared to the aforementioned RVE model (volume fraction is equal or less than 0.2), in accordance to the fact that in the dispersed system [42], higher volume fraction of the dispersed hard inclusions (the chitin fiber here) leads to a stiffer system [16,43]. It is also observable in Fig. 5 that the elastic moduli of chitin-protein composites are dependent on the length of chitin fiber in both dry and wet cases. As the length of chitin fiber increases from 5 nm to 20 nm, the elastic modulus of the composite system increases, corresponding to Eq. (1). Afterwards the elastic modulus reaches to a plateau (around 35 GPa in dry case and 25 GPa in wet case) as the length exceeds 20 nm, which is out of the description of Eq. (1). This phenomenon indicates a critical length of chitin

fiber for our composite model at around 20 nm. According to the scaling law in shear lag model [31], the critical stress should increase with length linearly when the length is shorter than critical length. Afterwards, when the length exceeds the critical length, the stress varies little. From large deformation test, we obtain that the strength (first peak stress during deformation) increases from 0.49 GPa to 1.14 GPa with 5 to 25 nm fiber length and finally hits the plateau of around 1.20 GPa with fiber length of 30 nm and 35 nm, as shown in Fig. 6. Our results fit well with this description. In reference to our chitin-protein composite model, the critical length of chitin fibers is within the range of 20-30 nm and the corresponding aspect ratio (length to width ratio) is around 12.

When water molecules occupy the space between chitin and protein, either positive or negative effect may be resulted. On one hand, the water molecules may act as the bridge to refine the hydrogen bond network, thus improving the integrity of the system [32]. On the other hand, water may block the bilayer interactions and diminish the adhesion strength [33]. How water molecules affect the system depends on the nature of the constituents of the system and the quantity of water molecules [32]. Here, we find that the number of hydrogen bonds formed between chitin and protein decreases as water molecules diffuse into the bilayer structure. From Fig. 3c and d, it is obvious that the dry sample contains more hydrogen bonds than the wet sample does in the outlined region, where the chitin-protein interaction is blocked by water molecules. Meanwhile, the bar chart in Fig. 5 shows the elastic modulus of dry samples are higher than that of wet case. This comparison corresponds to the study on the natural chitin-protein composite, the squid beaks. According to the experimental works on jumbo squid beaks [34,44], the dehydrated chitin-protein bio-composite exhibits higher elastic modulus compared to that in the hydrated state. In accordance with those studies, our simulations show that water

molecules have a negative effect on the elastic modulus of chitin-protein composite when the water content is around 16% in weight. Moreover, combining our simulations with the studies on chitin-protein interface [15,17], it is a reasonable inference that the lowered stiffness of the hydrated composite can be attributed to the weakening of the chitin-protein interface when water molecules are present. Nevertheless, noticing that the bilayer integrity can benefit from certain amount of water molecules [32], together with the fact that most natural chitin-based materials contain water, we expect that an optimal amount of water molecules may result a positive effect towards the chitin-protein system. It requires further examination on whether the water can act as the refining phase and what criteria makes water the refining phase in the chitin-protein composite system.

4.2. The zigzag structure between adjacent chitin layers

The periodic saw-tooth appearance is visible from the curves in Fig. 6. Such saw-tooth appearance becomes more obvious when the length of chitin fiber is longer than 15 nm. The stress increases to the peak, then quickly drops down and increases again. We plot the spacing displacement against chitin fiber length in Fig. 7. The displacement between adjacent stress peaks is around 1 nm, which could be regarded as a uniform feature for all modeled chitin-protein composites.

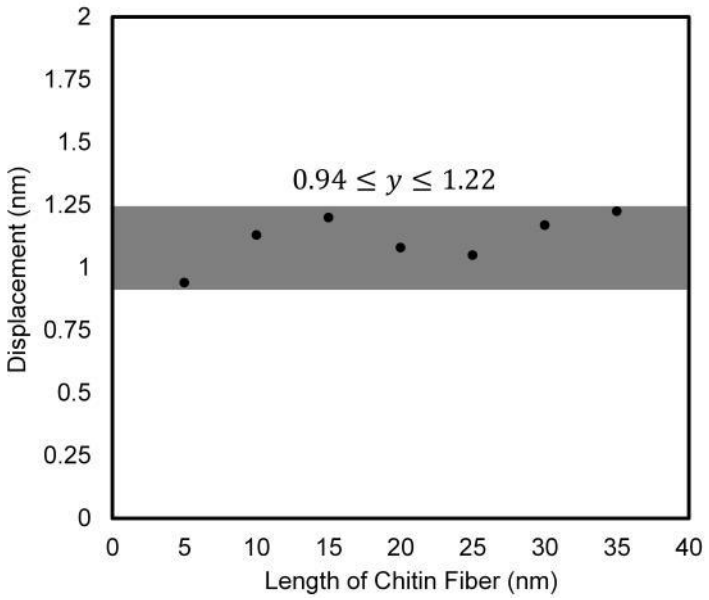

Fig. 7 The plot of spacing displacement against the length of chitin fiber. The upper and lower limits of *y* values in the shadowed region is 0.94 and 1.22 respectively.

The snapshots of adjacent chitin layers are captured during the large-strain deformation on 10 nm-chitin-fiber composite, as presented in Fig. 8. There exist many tooth-like structures, which are N-acetyl groups in chitin fibers as outlined in rectangles and the spacing distance between neighboring "teeth" is 1.04 nm.

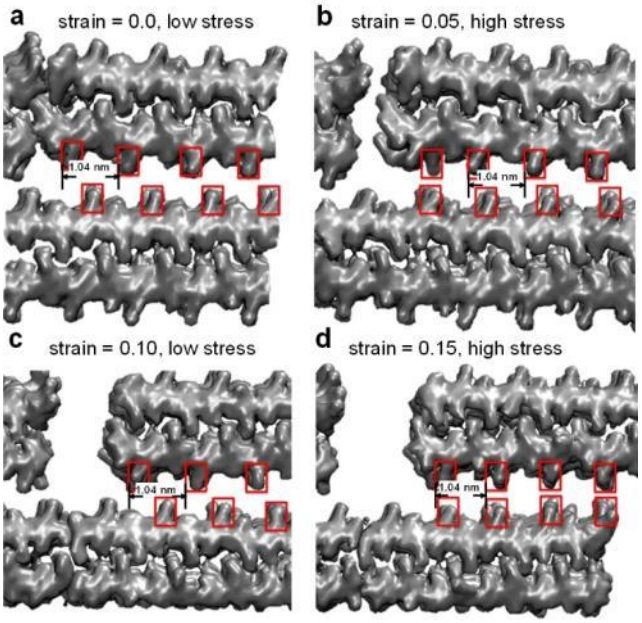

Fig. 8 a b c d Snapshots of adjacent chitin layers in chitin-protein composite, captured during large-strain tensile testing. Rectangles outline the "teeth" in chitin fibers, which are the acetyl group. Protein sheets that exist in between chitin fibers are eliminated

As shown in Fig. 8, the tooth-like structures interlock with each other at the initial state (*i.e.* strain is 0) where the stress and the potential energy are low. In Fig. 8b, these "teeth" face against each other in a tip-to-tip manner, leading to a high-stress state. Next in Fig. 8c the interlocked connections of adjacent chitin fibers are achieved again, corresponding to a low-energy state and the stress is relaxed. These snapshots illustrate that the composite undergoes low-to-high-stress (from Fig. 8a to Fig. 8b) and high-to-low-stress (from Fig. 8b to Fig. 8c) processes alternatively (from Fig. 8c to Fig. 8d) during the tensile testing. As the deformation proceeds, chitin fibers are pulled, stress increases and work of the external load is firstly stored in the elongated chitin fibers, afterwards, sliding between adjacent fibers occurs, the stored energy dissipates and stress in chitin fibers drops down. This relaxation process is achieved by losing one interlocked site as shown in Fig. 8a and c. These interlocked sites are similar to the

sacrificial bonds in biomaterials such as nacres, diatoms and bones [45-48]. In those materials the sacrificial bonds are folded proteins, which will unfold in response to pulling force, thus avoiding the fracture of other strong bonds in the material [45]. Here, in between the adjacent parallel chitin surfaces, the interlocked sites break sacrificially, which limits the stress accumulation in chitin fibers and therefore the chitin fibers are protected against fracture.

5. Conclusion

Atomistic models representing the chitin-protein nanocomposites are constructed following the design of tension-shear chain model. By performing molecular dynamics simulations, we conduct tensile tests and obtain elastic modulus and strength of these chitin-protein samples. The elastic modulus of chitin-protein composites drops by around 10 GPa (from 16-35 GPa to 9-25 GPa) with the presence of water (the water content is 16% in weight). Generally, longer embedded chitin fibers result in better mechanical performance for chitin-protein composite. Stiffness, strength and ductility of chitin-protein composites are optimized when the embedded chitin fibers are longer than 20 nm. Aside from that, we notice that the acetyl group in chitin acts as an interlocking unit between adjacent parallel chitin fibers, a pair of acetyl groups can combine together to form the interlocked site. When the composite is subjected to external loading, the binding sites can break sacrificially and protect the chitin fibers from fracture. Those interlocked sites are similar to the sacrificial bonds, which account for the strength and stiffness in many biological materials. The present molecular dynamics study on chitin-protein nanostructure is primarily based on the atomistic model. Future studies on larger-scale structures could be conducted using multi-scale modeling techniques (such as coarse grain modeling or finite element method) as well as advanced experimental programs, thus establish a linkage between structures and material properties at macroscopic length scale.

Acknowledgements

The authors are grateful to the support from Croucher Foundation through the Start-up Allowance for Croucher Scholars with the Grant No. 9500012, and the support from the Research Grants Council (RGC) in Hong Kong through the Early Career Scheme (ECS) with the Grant No. 139113.

References

1. Tharanathan RN, Kittur FS (2003) Chitin—the undisputed biomolecule of great potential. Critical Reviews in Food Science and Nutrition 43 (1):61-87
2. Ravi Kumar MN (2000) A review of chitin and chitosan applications. Reactive and functional polymers 46 (1):1--27
3. Krajewska B (2004) Application of chitin- and chitosan-based materials for enzyme immobilizations: a review. Enzyme and microbial technology 35 (2):126--139
4. Ehrlich H, Simon P, Carrillo-Cabrera W, Bazhenov VV, Botting JP, Ilan M, Ereskovsky AV, Muricy G, Worch H, Mensch A (2010) Insights into chemistry of biological materials: newly discovered silica-aragonite-chitin biocomposites in demosponges. Chemistry of Materials 22 (4):1462-1471
5. Chen PY, Lin AYM, Lin YS, Seki Y, Stokes AG, Peyras J, Olevsky EA, Meyers MA, McKittrick J (2008) Structure and mechanical properties of selected biological materials. Journal of the Mechanical Behavior of Biomedical Materials 1 (3):208-226. doi:http://dx.doi.org/10.1016/j.jmbbm.2008.02.003
6. Vincent JF, Wegst UG (2004) Design and mechanical properties of insect cuticle. Arthropod Structure & Development 33 (3):187--199
7. Miserez A, Li Y, Waite JH, Zok F (2007) Jumbo squid beaks: Inspiration for design of robust organic composites. Acta Biomaterialia 3 (1):139-149
8. Politi Y, Priewasser M, Pippel E, Zaslansky P, Hartmann J, Siegel S, Li C, Barth FG, Fratzl P (2012) A Spider's Fang: How to Design an Injection Needle Using Chitin-Based Composite Material. Advanced Functional Materials 22 (12):2519--2528
9. Sachs C, Fabritius H, Raabe D (2006) Experimental investigation of the elastic–plastic deformation of mineralized lobster cuticle by digital image correlation. Journal of Structural Biology 155 (3):409-425. doi:http://dx.doi.org/10.1016/j.jsb.2006.06.004
10. Romano P, Fabritius H, Raabe D (2007) The exoskeleton of the lobster Homarus americanus as an example of a smart anisotropic biological material. Acta Biomaterialia 3 (3):301-309. doi:http://dx.doi.org/10.1016/j.actbio.2006.10.003
11. Raabe D, Sachs C, Romano P (2005) The crustacean exoskeleton as an example of a structurally and mechanically graded biological nanocomposite material. Acta Materialia 53 (15):4281-4292. doi:http://dx.doi.org/10.1016/j.actamat.2005.05.027
12. Boßelmann F, Romano P, Fabritius H, Raabe D, Epple M (2007) The composition of the exoskeleton of two crustacea: The American lobster Homarus americanus and the edible crab Cancer pagurus. Thermochimica Acta 463 (1–2):65-68. doi:http://dx.doi.org/10.1016/j.tca.2007.07.018

13. Fabritius H-O, Sachs C, Triguero PR, Raabe D (2009) Influence of Structural Principles on the Mechanics of a Biological Fiber-Based Composite Material with Hierarchical Organization: The Exoskeleton of the Lobster Homarus americanus. Advanced Materials 21 (4):391-400. doi:10.1002/adma.200801219
14. Al-Sawalmih A, Li C, Siegel S, Fabritius H, Yi S, Raabe D, Fratzl P, Paris O (2008) Microtexture and Chitin/Calcite Orientation Relationship in the Mineralized Exoskeleton of the American Lobster. Advanced Functional Materials 18 (20):3307-3314. doi:10.1002/adfm.200800520
15. Jin K, Feng X, Xu Z (2013) Mechanical Properties of Chitin–Protein Interfaces: A Molecular Dynamics Study. BioNanoScience 3 (3):312-320. doi:10.1007/s12668-013-0097-2
16. Nikolov S, Petrov M, Lymperakis L, Friák M, Sachs C, Fabritius H-O, Raabe D, Neugebauer J (2010) Revealing the Design Principles of High-Performance Biological Composites Using *Ab initio* and Multiscale Simulations: The Example of Lobster Cuticle. Advanced Materials 22 (4):519--526
17. Yu Z, Xu Z, Lau D (2014) Effect of Acidity on Chitin–Protein Interface: A Molecular Dynamics Study. BioNanoScience:DOI: 10.1007/s12668-12014-10138-12665
18. Yu Z, Lau D (2015) Development of a coarse-grained α-chitin model on the basis of MARITINI forcefield. Journal of Molecular Modeling, 21 (5):128
19. Petrov M, Lymperakis L, Friák M, Neugebauer J (2013) *Ab Initio* Based conformational study of the crystalline α-chitin. Biopolymers 99 (1):22--34
20. Sachs C, Fabritius H, Raabe D (2006) Hardness and elastic properties of dehydrated cuticle from the lobster Homarus americanus obtained by nanoindentation. Journal of Materials Research 21 (08):1987-1995. doi:doi:10.1557/jmr.2006.0241
21. Sachs C, Fabritius H, Raabe D (2008) Influence of microstructure on deformation anisotropy of mineralized cuticle from the lobster Homarus americanus. Journal of Structural Biology 161 (2):120-132. doi:http://dx.doi.org/10.1016/j.jsb.2007.09.022
22. Raabe D, Romano P, Sachs C, Fabritius H, Al-Sawalmih A, Yi SB, Servos G, Hartwig HG (2006) Microstructure and crystallographic texture of the chitin–protein network in the biological composite material of the exoskeleton of the lobster Homarus americanus. Materials Science and Engineering: A 421 (1–2):143-153. doi:http://dx.doi.org/10.1016/j.msea.2005.09.115
23. Ji B, Gao H (2004) Mechanical properties of nanostructure of biological materials. Journal of the Mechanics and Physics of Solids 52 (9):1963-1990
24. Gao H, Ji B, Jäger IL, Arzt E, Fratzl P (2003) Materials become insensitive to flaws at nanoscale: lessons from nature. Proceedings of the national Academy of Sciences 100 (10):5597-5600
25. Ji B, Gao H (2010) Mechanical principles of biological nanocomposites. Annual Review of Materials Research 40:77-100
26. Dunlop JW, Fratzl P (2013) Multilevel architectures in natural materials. Scripta Materialia 68 (1):8-12
27. Jäger I, Fratzl P (2000) Mineralized collagen fibrils: a mechanical model with a staggered arrangement of mineral particles. Biophysical Journal 79 (4):1737-1746
28. Sinko R, Mishra S, Ruiz L, Brandis N, Keten S (2013) Dimensions of Biological Cellulose Nanocrystals Maximize Fracture Strength. ACS Macro Letters 3:64-69
29. Keten S, Xu Z, Ihle B, Buehler MJ (2010) Nanoconfinement controls stiffness, strength and mechanical toughness of β-sheet crystals in silk. Nature materials 9 (4):359-367
30. Nova A, Keten S, Pugno NM, Redaelli A, Buehler MJ (2010) Molecular and nanostructural mechanisms of deformation, strength and toughness of spider silk fibrils. Nano Letters 10 (7):2626-2634

31. Chen B, Wu PD, Gao H (2009) A characteristic length for stress transfer in the nanostructure of biological composites. Composites Science and Technology 69 (7–8):1160-1164. doi:http://dx.doi.org/10.1016/j.compscitech.2009.02.012
32. Compton OC, Cranford SW, Putz KW, An Z, Brinson LC, Buehler MJ, Nguyen ST (2012) Tuning the mechanical properties of graphene oxide paper and its associated polymer nanocomposites by controlling cooperative intersheet hydrogen bonding. ACS nano 6 (3):2008-2019
33. Lau D, Büyüköztürk O, Buehler MJ (2012) Characterization of the intrinsic strength between epoxy and silica using a multiscale approach. Journal of Materials Research 27 (14):1787--1796
34. Miserez A, Schneberk T, Sun C, Zok FW, Waite JH (2008) The transition from stiff to compliant materials in squid beaks. Science 319 (5871):1816-1819
35. Sikorski P, Hori R, Wada M (2009) Revisit of α-chitin crystal structure using high resolution X-ray diffraction data. Biomacromolecules 10 (5):1100--1105
36. Humphrey W, Dalke A, Schulten K (1996) VMD: visual molecular dynamics. Journal of molecular graphics 14 (1):33--38
37. Plimpton S (1995) Fast parallel algorithms for short-range molecular dynamics. Journal of Computational Physics 117 (1):1-19
38. Guvench O, Mallajosyula SS, Raman EP, Hatcher E, Vanommeslaeghe K, Foster TJ, Jamison FW, MacKerell Jr AD (2011) CHARMM Additive All-Atom Force Field for Carbohydrate Derivatives and Its Utility in Polysaccharide and Carbohydrate--Protein Modeling. Journal of chemical theory and computation 7 (10):3162--3180
39. Huang J, MacKerell AD (2013) CHARMM36 all-atom additive protein force field: Validation based on comparison to NMR data. Journal of computational chemistry 34 (25):2135--2145
40. Beckham GT, Crowley MF (2011) Examination of the α-chitin structure and decrystallization thermodynamics at the nanoscale. The Journal of Physical Chemistry B 115 (15):4516--4522
41. Mori T, Tanaka K (1973) Average stress in matrix and average elastic energy of materials with misfitting inclusions. Acta metallurgica 21 (5):571-574
42. Torquato S (1998) Effective stiffness tensor of composite media: II. Applications to isotropic dispersions. Journal of the Mechanics and Physics of Solids 46 (8):1411-1440
43. Nikolov S, Fabritius H, Petrov M, Friák M, Lymperakis L, Sachs C, Raabe D, Neugebauer J (2011) Robustness and optimal use of design principles of arthropod exoskeletons studied by *ab initio*-based multiscale simulations. Journal of the mechanical behavior of biomedical materials 4 (2):129-145
44. Miserez A, Rubin D, Waite JH (2010) Cross-linking chemistry of squid beak. Journal of Biological Chemistry 285 (49):38115--38124
45. Smith BL, Schäffer TE, Viani M, Thompson JB, Frederick NA, Kindt J, Belcher A, Stucky GD, Morse DE, Hansma PK (1999) Molecular mechanistic origin of the toughness of natural adhesives, fibres and composites. Nature 399 (6738):761-763
46. Gebeshuber IC, Kindt JH, Thompson JB, Del Amo Y, Stachelberger H, Brzezinski MA, Stucky GD, Morse DE, Hansma PK (2003) Atomic force microscopy study of living diatoms in ambient conditions. Journal of Microscopy 212 (3):292-299. doi:10.1111/j.1365-2818.2003.01275.x
47. Dugdale TM, Dagastine R, Chiovitti A, Mulvaney P, Wetherbee R (2005) Single Adhesive Nanofibers from a Live Diatom Have the Signature Fingerprint of Modular Proteins. Biophysical Journal 89 (6):4252-4260. doi:http://dx.doi.org/10.1529/biophysj.105.062489

48. Sarkar A, Caamano S, Fernandez JM (2007) The Mechanical Fingerprint of a Parallel Polyprotein Dimer. Biophysical Journal 92 (4):L36-L38. doi:http://dx.doi.org/10.1529/biophysj.106.097741